

# TOTAL VARIATION SUPER-RESOLUTION FOR 3D TRABECULAR BONE MICRO-STRUCTURE SEGMENTATION

Alina Toma<sup>1</sup>, Loïc Denis<sup>2</sup>, Bruno Sixou<sup>1</sup>, Jean-Baptiste Pialat<sup>3</sup>, Françoise Peyrin<sup>1,4</sup>

<sup>1</sup> CREATIS, INSA de Lyon, Inserm U1044, CNRS UMR 5220,  
Université Lyon 1, Université de Lyon, 69621 Lyon, France

<sup>2</sup> LaHC, CNRS UMR 5516, Université de Saint-Etienne, 42000 Saint-Etienne, France

<sup>3</sup> Inserm U1033; Université de Lyon, Hospices Civils de Lyon, 69437 Lyon, France

<sup>4</sup> ESRF, Imaging Group, 38043 Grenoble Cedex, France

## ABSTRACT

The analysis of the trabecular bone micro-structure plays an important role in studying bone fragility diseases such as osteoporosis. In this context, X-ray CT techniques are increasingly used to image bone micro-architecture. The aim of this paper is to improve the segmentation of the bone micro-structure for further bone quantification. We propose a joint super-resolution/segmentation method based on total variation with a convex constraint. The minimization is performed with the Alternating Direction Method of Multipliers (ADMM). The new method is compared with the bicubic interpolation method and the classical total variation regularization. All methods were tested on blurred, noisy and down-sampled 3D synchrotron micro-CT bone volumes. Improved segmentation is obtained with the proposed joint super-resolution/segmentation method.

**Index Terms**— segmentation, super-resolution, 3D trabecular micro-structure, TV regularization, CT images.

## 1. INTRODUCTION

X-Ray micro-CT provides 3D images at spatial resolution higher than clinical CT systems. It has been particularly used to analyze bone micro-architecture in the study of osteoporosis, a bone fragility disease, still difficult to diagnose [1]. Bone micro-architecture which is an important determinant of biomechanical strength is made of a complex arrangement of thin structures called trabeculae, having a thickness around 150  $\mu\text{m}$ . The 3D images of bone micro-architecture obtained by X-Ray micro-CT are further processed to extract 3D quantitative descriptors of the bone micro-structure. Bone structure analysis requires an image segmentation method as a first step to extract the bone from the background. Then the calculation of 3D morphometric parameters such as the bone vol-

ume to total volume ratio, mean trabecular thickness, mean trabecular spacing but also topological parameters such as the connectivity or the organization of the micro-structure in plate or rods [2, 3] is considered. Such descriptors have been reported in many studies but limited to the analysis of *ex vivo* bone samples. While the spatial resolution of clinical CT scanners is not sufficient to resolve the trabecular structure, new High Resolution peripheral Quantitative CT (HR-pQCT) systems have been commercialized to investigate bone micro-architecture *in-vivo* at peripheral sites (tibia and radius) [4]. After imaging, the 3D images are segmented and the same parameters than those used in X-ray micro-CT are calculated to quantify the bone micro-architecture of patients. However, the result of image segmentation can be poor, compromising the subsequent quantification [5]. This problem is related to the limited physical spatial resolution of the HR-pQCT which is close to the trabecular thickness. In this paper, we propose a 3D super-resolution method in view to improve the segmentation of low-resolution volumes of bone micro-structure.

Image segmentation has been widely studied in the literature, see for example [6–9]. Image super-resolution is also an active research field [10, 11]. Yet, in most studies, image restoration (denoising, deblurring, super-resolution) and image segmentation are considered separately. Recent work on convex relaxation of segmentation problems have proved that some segmentation models could be exactly computed by resorting to techniques similar to total variation denoising methods [9, 12]. This bridges the gap between the families of segmentation methods and restoration methods and offers attractive theoretical guarantees of global minimization, thus segmentation results that are independent from the initialization. By generalizing these segmentation methods to linear degradations such as blur, it is possible to perform joint restoration and segmentation, as shown in a very recent work [13].

Since the images we are interested in display quasi-binary structures, we can strongly rely on a total variation (TV) prior model and consider single-image super-resolution. We compare segmentation of a grayscale volume obtained by a TV

This work was supported by the LABEX PRIMES (ANR-11-LABX-0063) of Université de Lyon, within the program "Investissements d'Avenir" (ANR-11-IDEX-0007) operated by the French National Research Agency (ANR).

regularized super-resolution method with joint segmentation / super-resolution on volumes simulated from a ground-truth segmentation obtained with high-resolution micro-CT.

The paper is organized as follows. In the first part, we formulate the joint segmentation / super-resolution problem as a linear inverse problem, following the approach of Paul *et al.* [13]. We detail how to perform the minimization of the regularization functional using the Alternating Direction Method of Multipliers (ADMM) which is one of the state-of-the-art methods for TV regularization [14–16]. Then, the validation of the proposed approach is performed on experimental high-resolution micro-CT volumes of bone samples at 20  $\mu\text{m}$  after simulating the effect of a loss of spatial resolution and degradation by noise and blur. Concluding remarks are given in the last section.

## 2. SUPER-RESOLUTION SEGMENTATION

### 2.1. Convex formulation

The reconstruction of a 3D image with an improved resolution from a single low-resolution volume requires a model of the degradation the volume undergoes during the acquisition process. Starting from a high-resolution volume  $\mathbf{f}$ , the low-resolution volume  $\mathbf{g}$  can be modeled as resulting from a blurring followed by a down-sampling, with some added random fluctuations to account for different sources of noise:

$$\mathbf{g} = \mathbf{A}\mathbf{f} + \mathbf{w}, \quad (1)$$

where  $\mathbf{g} \in \mathbb{R}^N$  denotes the  $N$ -voxels low-resolution volume measured by the imaging system,  $\mathbf{f} \in \mathbb{R}^{N'}$  denotes an  $N' = N \times p^3$ -voxels high-resolution volume with super-resolution factor  $p$  in each of the 3 dimensions of the volume,  $\mathbf{A}$  is the linear operator accounting for blurring followed by down-sampling and  $\mathbf{w}$  is the (random) noise component.

Reconstruction of a higher-resolution volume  $\hat{\mathbf{f}}$  from the low-resolution volume  $\mathbf{g}$  requires to solve a linear inverse problem. Maximum *a posteriori* restoration methods are widely used. They define the high-resolution volume  $\hat{\mathbf{f}}$  as the solution of least cost:

$$\hat{\mathbf{f}} \in \arg \min_{\mathbf{f}} \frac{\mu}{2} \|\mathbf{A}\mathbf{f} - \mathbf{g}\|_2^2 + \mathcal{R}(\mathbf{f}), \quad (2)$$

where the first term of the sum penalizes misfit between the reconstructed volume  $\mathbf{f}$  and the data  $\mathbf{g}$  (i.e., the negative of the log-likelihood under a stationary white Gaussian noise hypothesis),  $\mathcal{R}(\cdot)$  is a regularization term (i.e., prior term) that favors smooth reconstructions and  $\mu$  is inversely proportional to the noise variance and balances the relative weight of each of the two terms.

Total variation (TV) is a classical regularization functional used to restore images with sharp edges [17]. The isotropic total variation of a function  $f$  is defined as the  $L_1$  norm of its gradient:  $\mathcal{R}_{\text{TV}}(f) = \int \|\nabla f(\mathbf{r})\| d\mathbf{r}$ , where  $\|\nabla f(\mathbf{r})\|$  is the Euclidean norm of the gradient. When a

discrete volume  $\mathbf{f}$  is considered, TV can be rewritten under the form:

$$\mathcal{R}_{\text{TV}}(\mathbf{f}) = \sum_i \|D_i \mathbf{f}\|, \quad (3)$$

where the sum is carried over all voxels of  $\mathbf{f}$  and  $D_i$  is the discrete gradient operator at voxel  $i$ .

In a two-phase segmentation task, each voxel of the segmented image  $s$  is assigned to one of the two phases. Let  $c_0$  and  $c_1$  be the average graylevels of each phase. A satisfying segmentation of image  $f$  is a labelling such that each voxel is assigned to a phase whose average graylevel is close to the corresponding graylevel of image  $\mathbf{f}$  and where neighbor voxels most often belong to the same class. One can thus consider the following functional first proposed by Mumford and Shah [18]:

$$\int_{\mathcal{R}_0} [f(\mathbf{r}) - c_0]^2 d\mathbf{r} + \int_{\mathcal{R}_1} [f(\mathbf{r}) - c_1]^2 d\mathbf{r} + \nu|\Gamma| \quad (4)$$

where  $\mathcal{R}_0$  and  $\mathcal{R}_1$  are the regions of each of the two phases and  $|\Gamma|$  denotes the perimeter of the boundary between regions  $\mathcal{R}_0$  and  $\mathcal{R}_1$ . In discrete form, minimizing this cost function corresponds to the following minimization problem:

$$\arg \min_{\mathbf{s} \in \mathbb{B}} \frac{\mu}{2} \|\mathbf{f} - \mathbf{s}\|_2^2 + \mathcal{R}_{\text{TV}}(\mathbf{s}) \quad (5)$$

where  $\mathbb{B} = \{c_0, c_1\}^{N'}$  is the set of all  $N'$ -voxels two-phase volumes and  $\mu = 2|c_1 - c_0|/\nu$ .

In order to perform joint super-resolution and segmentation, we consider the following optimization problem:

$$\arg \min_{\mathbf{s} \in \mathbb{B}} \frac{\mu}{2} \|\mathbf{A}\mathbf{s} - \mathbf{g}\|_2^2 + \mathcal{R}_{\text{TV}}(\mathbf{s}). \quad (6)$$

Minimization problem (6) is NP-hard for general linear operators  $\mathbf{A}$ . We therefore only perform approximate minimization by considering instead the following convex relaxation:

$$\hat{\mathbf{s}} \in \arg \min_{\mathbf{s} \in [c_0, c_1]^{N'}} \frac{\mu}{2} \|\mathbf{A}\mathbf{s} - \mathbf{g}\|_2^2 + \mathcal{R}_{\text{TV}}(\mathbf{s}), \quad (7)$$

where the set of two-phase volumes has been replaced by the convex set of graylevel volumes with graylevels in the range  $[c_0, c_1]$ .

### 2.2. The alternate direction of minimization method

Restoration of a high-resolution image  $\hat{\mathbf{s}}$  from a single low-resolution image requires solving an optimization problem of the form of equation (7). By introducing auxiliary variables, the minimization problem can be re-expressed as:

$$\hat{\mathbf{s}} \in \arg \min_{\mathbf{s}, \{\mathbf{h}_i\}, \mathbf{k} \in [c_0, c_1]^{N'}} \frac{\mu}{2} \|\mathbf{A}\mathbf{s} - \mathbf{g}\|_2^2 + \sum_i \|\mathbf{h}_i\|, \quad (8)$$

s.t.  $\forall i, \mathbf{h}_i = D_i \mathbf{s}$ , and  $\mathbf{k} = \mathbf{s}$ .

The optimization problem (8) can be solved efficiently by finding the saddle point of the augmented Lagrangian using the alternating direction method of multipliers (ADMM) [14–16]. The augmented Lagrangian associated to constrained problem (8) writes:

$$\begin{aligned} \mathcal{L}_A(\mathbf{s}, \{\mathbf{h}_i\}, \mathbf{k}, \{\boldsymbol{\lambda}_i\}, \boldsymbol{\lambda}_C) = & \frac{\mu}{2} \|\mathbf{A}\mathbf{s} - \mathbf{g}\|_2^2 + \sum_i \|\mathbf{h}_i\| \quad (9) \\ & + \sum_i \left[ \frac{\beta}{2} \|\mathbf{h}_i - \mathbf{D}_i \mathbf{s}\|^2 - \boldsymbol{\lambda}_i^t (\mathbf{h}_i - \mathbf{D}_i \mathbf{s}) \right] \\ & + \mathbf{I}_C(\mathbf{k}) + \frac{\beta}{2} \|\mathbf{k} - \mathbf{s}\|_2^2 - \boldsymbol{\lambda}_C^t (\mathbf{k} - \mathbf{s}) \end{aligned}$$

with  $\boldsymbol{\lambda}_i$  the Lagrange multipliers for the  $i^{\text{th}}$  equality constraint,  $\boldsymbol{\lambda}_C$  the Lagrange multiplier for convex constraint and  $\mathbf{I}_C(\mathbf{k})$  is the indicator function of the convex set  $\mathbf{C} = [c_0, c_1]^{N'}$ .

The ADMM method alternates between five updates:

1. Update of the high-resolution reconstruction  $\mathbf{s}$ , by (approximately) solving the linear system:

$$\mathbf{H}\mathbf{s}^{(k+1)} = \mu \mathbf{A}^t \mathbf{g} + \sum_i \mathbf{D}_i^t (\beta \mathbf{h}_i^{(k)} - \boldsymbol{\lambda}_i^{(k)}) + \beta \mathbf{k} - \boldsymbol{\lambda}_C,$$

with  $\mathbf{H} = \mu \mathbf{A}^t \mathbf{A} + \beta \mathbf{I} + \sum_i \beta \mathbf{D}_i^t \mathbf{D}_i$ .

2. Update of the auxiliary variables  $\mathbf{h}_i$ , by applying a soft-thresholding operator  $\mathcal{S}_\beta$ :

$$\mathbf{h}_i^{(k+1)} = \mathcal{S}_\beta \left( \mathbf{D}_i \mathbf{s}^{(k+1)} + \boldsymbol{\lambda}_i^{(k)} / \beta \right),$$

with  $\mathcal{S}_\beta(\mathbf{u}) = \max \left( 1 - \frac{1}{\beta \|\mathbf{u}\|}, 0 \right) \cdot \mathbf{u}$ .

3. Update of the auxiliary variable  $\mathbf{k}$ :

$$\mathbf{k}^{(k+1)} = \pi_C \left( \mathbf{s}^{(k)} + \frac{\boldsymbol{\lambda}_C^{(k)}}{\beta} \right),$$

where  $\pi_C$  is the projection on the convex set  $\mathbf{C}$ .

4. Update of the Lagrange multipliers  $\boldsymbol{\lambda}_i$ :

$$\boldsymbol{\lambda}_i^{(k+1)} = \boldsymbol{\lambda}_i^{(k)} - \beta \left( \mathbf{h}_i^{(k+1)} - \mathbf{D}_i \mathbf{s}^{(k+1)} \right).$$

5. Update of the Lagrange multiplier  $\boldsymbol{\lambda}_C$ :

$$\boldsymbol{\lambda}_C^{(k+1)} = \boldsymbol{\lambda}_C^{(k)} - \beta \left( \mathbf{k}^{(k+1)} - \mathbf{s}^{(k+1)} \right).$$

For comparison purposes, we will also consider in the next part the super-resolution with the model of equations (2)-(3), i.e. without the box constraints. This appears as a special case of the algorithm just described.

### 3. NUMERICAL EXPERIMENTS

#### 3.1. Implementation details

We applied the two total variation based regularizations and the bicubic interpolation method to experimental data. Human bone samples (cylinder core of 10mm) were scanned

with parallel-beam synchrotron micro-CT at 10  $\mu\text{m}$ . To this aim, 1500 2D projections were acquired after rotating the sample. The 3D images were reconstructed using the Filtered back projection algorithm [19] and further resampled at 20  $\mu\text{m}$ . Due to the high signal to noise ratio of synchrotron CT images, the binary volume of the bone structure was obtained by simple thresholding. This binary image of size  $328 \times 328 \times 328$  is considered as the ground truth and is shown in Fig. 1. The low resolution volumes were obtained considering a sub-sampling rate of  $p = 2$ . For the blurring operation, we have used a Gaussian point spread function of standard deviation  $\sigma_{blur} = 2.425$ . We tested two additive Gaussian noise levels with standard deviations  $\sigma = 0.01$  and  $\sigma = 0.1$ .

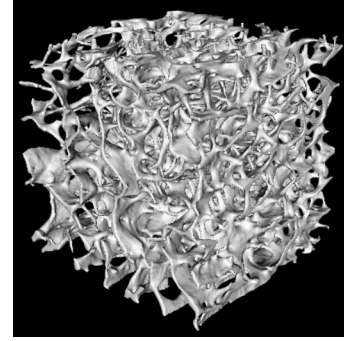
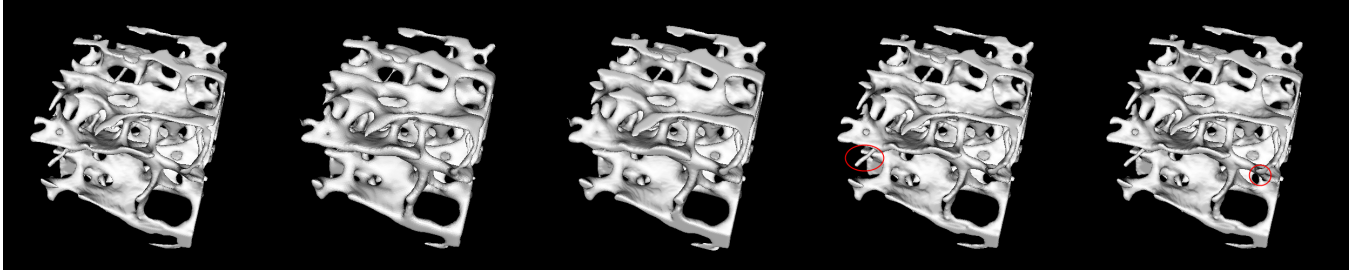


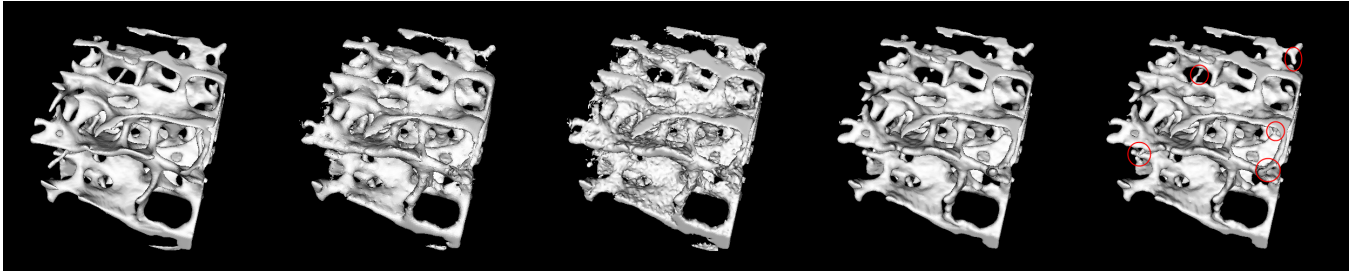
Fig. 1. The reference binary volume.

To ensure the convergence of the regularization methods, we considered the following stopping criteria of the ADMM iterations:  $\frac{\|f^{(k-1)} - f^{(k)}\|_2}{\|f^{(k)}\|_2} < \epsilon$  with  $\epsilon = 10^{-4}$  for the noise level  $\sigma = 0.01$  and  $\epsilon = 5 \cdot 10^{-4}$  for  $\sigma = 0.1$ . A high resolution volume was obtained from the low-resolution, blurred and noisy volume with TV and TV with box constraints regularization. An extensive sweeping of the regularization parameters was performed in order to show that TV based regularizations can be useful to recover the high resolution segmented ground truth. For a fixed regularization parameter, the  $\beta$  parameter is chosen beforehand by computing only a limited number of iterations and in order to have the fastest decrease of the regularization functional. For each method, the regularization parameter  $\mu$  chosen is the one that maximizes the DICE [20] value between the binary ground truth and the segmented reconstructed volume obtained with the threshold 0.5. For comparison reasons, the low resolution volume and the bicubic interpolation volume were segmented with Otsu's method [21], for both noise levels. The performance of the methods was measured considering the DICE value and also the quantitative bone micro-architecture parameters such as the bone volume to total volume (BTVV in %), the Euler number ( $\chi$ ) [22] and the density of connectivity (dconn in  $\text{mm}^{-3}$ ), normalizing the connectivity ( $\beta_1$ ) by the total volume, where  $\beta_1 = \beta_0 + \beta_2 - \chi$  and  $\beta_0, \beta_2$  are the number of the connected components and the number of cavities [23].



(a) Ground-truth volume (b) Low resolution volume (c) Bicubic interpolation (d) TV regularization (e) TVbox regularization

**Fig. 2.** Comparison of 3D restoration methods for the noise level  $\sigma=0.01$ .



(a) Ground-truth volume (b) Low resolution volume (c) Bicubic interpolation (d) TV regularization (e) TVbox regularization

**Fig. 3.** Comparison of 3D restoration methods for the noise level  $\sigma=0.1$ .

### 3.2. Results

Crops of size  $150 \times 150 \times 150$  of the resulted binary volumes are shown in Fig. 2 for the noise level  $\sigma = 0.01$  and in Fig. 3 for  $\sigma = 0.1$ . From these images we can visually estimate that the TV based methods are better recovering the bone structure and that TVbox method is the preferred method for solving our problem. The same conclusion can be taken from Fig. 4 that shows a slice of the ground-truth volume, of the low resolution gray level volume and of the resulted binary volumes with the tested method. The quantitative results are summarized in Table 1. From this table we can see the efficiency of the TV regularization methods. The TV methods outperforms clearly the interpolation method which gives poor estimates of the structural parameters. The DICE, Euler number, connectivity, density of connectivity, and BTVT are all improved with the TV based regularization approaches.

The best reconstruction results and structural parameters are obtained with additional box constraint (TVbox method).

### 4. CONCLUSION

In this paper, we proposed a super-resolution segmentation method based on the total variation regularization with convex constraint and ADMM minimization for improving the further trabecular bone micro-structure quantification from micro-CT volumes. We compared this new approach with a standard interpolation method and TV super-resolution method on noisy, blurred, low-resolution volumes in terms of DICE and structural parameters. Better results are obtained

when a convex constraint is included in the TV regularization functional. We observe that the bone volume to total volume is nearly well restored and that the connectivity is also improved compared to the original. In further studies, we will consider solving the optimization problem without requiring the inversion of the linear operators involved in the cost function as in [24]. In the practical situation where the ground truth is not known, we will address the choice of the regularization parameters with methods such as Morozov principle. Also, larger data set will be considered to validate our conclusion.

### REFERENCES

- [1] E. Seeman and P. D. Delmas, "Bone quality—the material and structural basis of bone strength and fragility", *N. Engl. J. Med.*, vol. 354, no. 21, pp. 2250-61, 2006.
- [2] T. Hildebrand, A. Laib, R. Muller, J. Dequeker and P. Rueggsegger, "Direct three-dimensional morphometric analysis of human cancellous bone: microstructural data from spine, femur, iliac crest, and calcaneus", *J. Bone Miner. Res.*, vol. 14, no. 7, pp. 1167-74, 1999.
- [3] F. Peyrin, D. Attali, C. Chappard and C. L. Benhamou "Local plate/rod descriptors of 3D trabecular bone micro-CT images from medial axis topologic analysis", *Med. Phys.*, vol. 37, no. 8, pp. 4364-76, 2010.
- [4] S. Boutroy, M. L. Bouxsein, F. Munoz and P. D. Delmas, "In vivo assessment of trabecular bone microarchitecture by high-resolution peripheral quantitative computed tomography", *J. Clin. Endocrinol. Metab.*, vol. 90, no. 12, pp. 6508-15, 2005.
- [5] W. Tjong, G. J. Kazakia, A. J. Burghardt and S. Majumdar, "The effect of voxel size on high-resolution peripheral

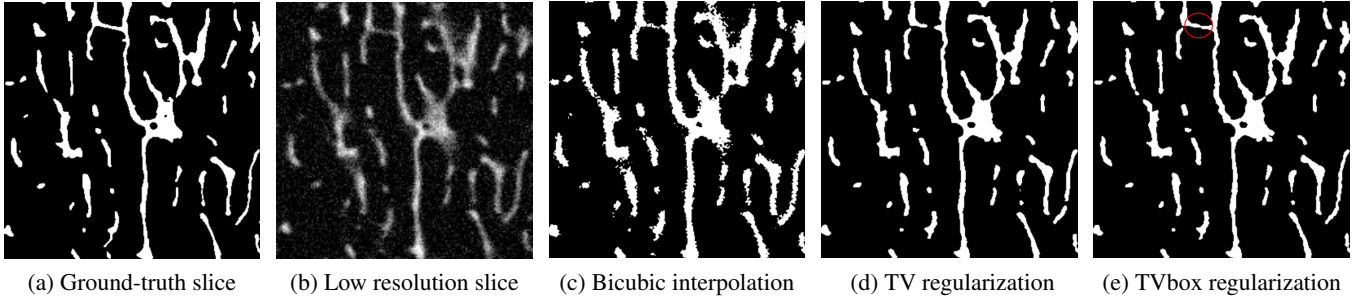


Fig. 4. Slice of the restored volumes for the noise level  $\sigma=0.1$ .

Parameter	Reference	$\sigma = 0.01$				$\sigma = 0.1$			
		Low res.	Bicubic Interp.	TV	TVbox	Low res.	Bicubic Interp.	TV	TVbox
<b>DICE</b>	1	-	0.778	0.962	<b>0.970</b>	-	0.773	0.898	<b>0.906</b>
<b>Euler no.</b>	-1211	-1006	-1006	-1018	<b>-1106</b>	4888	11201	-686	<b>-723</b>
<b>dconn (mm<sup>-3</sup>)</b>	4.86	3.99	4.01	4.45	<b>4.52</b>	16.61	11.98	3.92	<b>4.20</b>
<b>BTV (%)</b>	11.07	16.86	16.76	11.23	<b>11.14</b>	16.48	16.38	11.78	<b>11.52</b>

Table 1. Quantitative parameters for two noise levels ( $\sigma = 0.01$  and  $\sigma = 0.1$ )

computed tomography measurements of trabecular and cortical bone microstructure”, *Med. Phys.*, vol. 39, no. 4, pp. 1893-903, Apr. 2012.

- [6] T. F. Chan and J. J. Shen, "Image processing and analysis: Variational, PDE, wavelet and stochastic methods", Philadelphia: Society for Industrial and Applied Mathematics, 2005.
- [7] T. F. Chan and L. Vese, "Active contours without edges", *IEEE Trans. Image Process.*, vol. 10, no. 2, pp. 266-77, 2001.
- [8] D. Cremers, M. Rousson and R. Deriche, "A review of statistical approaches to level set segmentation: Integrating color, texture, motion and shape", *Int. J. Comput. Vis.*, vol. 72, pp. 195-215, 2007.
- [9] T. Goldstein, X. Bresson and S. Osher, "Geometric applications of the split Bregman method: segmentation and surface reconstruction", *J. Sci. Comput.*, vol. 45, pp. 272-93, 2010.
- [10] S.D.Babacan, R.Molina and A.K.Katsaggelos, "Total Variation Super Resolution Using A Variational Approach", *Proc. Int. Conf. Image Process.*, 2008, pp. 641-44.
- [11] Z. Ren, C. He and Q. Zhang, "Fractional order total variation regularization for image super-resolution", *Signal Process.*, vol. 93, no. 9, pp. 2408-21, 2013.
- [12] T. F. Chan, S. Esedoglu, and M. Nikolova, "Algorithms for Finding Global Minimizers of Image Segmentation and Denoising Models", *SIAM J. Appl. Math.* vol. 66, no. 5, pp. 1632-48, 2006.
- [13] G. Paul, J. Cardinale and I. F. Sbalzarini, "Coupling image restoration and segmentation: A generalized linear model/Bregman perspective", *Int. J. Comput. Vis.*, vol. 104, pp. 69-93, 2013.
- [14] J. Yang, W. Yin, Y. Zhang and Y. Wang, "A fast algorithm for edge-preserving variational multichannel image restoration", *SIAM J. Imaging Sci.*, vol. 2, pp.569-92, 2008.
- [15] M. Afonso, J. Bioucas-Dias and M. Figueiredo, "Fast image recovery using variable splitting and constrained optimization", *IEEE Trans. Image Process.*, vol. 19, pp. 2345-56, 2010.
- [16] MK. Ng, P. Weiss and X. Yuan, "Solving constrained total-variation image restoration and reconstruction problems via alternating direction methods", *SIAM J. Sci. Comput.*, vol. 32, pp. 2710-36, 2010.
- [17] L. I. Rudin, S. Osher and E. Fatemi, "Nonlinear total variation based noise removal algorithms", *Phys.D*, vol. 60, pp. 259-68, 1992.
- [18] D. Mumford and J. Shah, "Optimal approximations by piecewise smooth functions and associated variational problems", *Comm. Pure Appl. Math.*, vol. 42, pp. 577-685, July 1989.
- [19] M. Salome, F. Peyrin, P. Cloetens, C. Odet, A. M. Laval-Jeantet, J. Baruchel and P. Spanne, "A synchrotron radiation microtomography system for the analysis of trabecular bone samples", *Med. Phys.*, vol. 26, no. 10, pp. 2194 -204, 1999
- [20] L. R. Dice, "Measures of the amount of ecologic association between species", *Ecology*, vol. 26, no.3, pp. 297-302, 1945.
- [21] N. Otsu, "A threshold selection method from gray-level histograms", *IEEE Trans. Sys., Man, Cyber.*, vol. 9, no.1, pp. 62-66, 1979.
- [22] J. Ohser, W. Nagel and K. Schloditz, "Miles formulae for boolean models observed on lattices", *Image Anal. Stereol.*, vol. 28, no. 2, pp. 77-92, 2009.
- [23] A. Odgaard, "Three-dimensional methods for quantification of cancellous bone architecture", *Bone*, vol 20, no. 4, pp. 315-28, 1997.
- [24] L. Condat, "A primal-dual Splitting Method for Convex Optimization Involving Lipschitzian, Proximinal and Linear Composite Terms", *J. Optim. Theory. Appl.*, vol. 158, no. 2, pp. 460-79, 2013.